Interface-Dependent Efficiency Tradeoff in Si-Based Carrier-Selective Solar Cells

Nithin Chatterji, Aldrin Antony, and Pradeep R. Nair

***Abstract*— Carrier-selective (CS) silicon solar cells are of recent research interest, and a variety of different materials have been investigated in this regard. However, the efficiency tradeoff with CS material/interface properties is not yet fully explored. In this context, through detailed analytical and numerical modeling, here we provide several interesting insights on the same. First, we show that perfect band alignment is a desirable feature only if the interface is devoid of any trap states. Otherwise, a band offset of around 0.2–0.4 eV provides sufficient band bending to reduce the effect of interface recombination, thus improving the performance. Surprisingly, the interface passivation quality for the minority carrier extraction layer is found to be far less demanding than that for the majority carrier extraction layer. In addition, doping density and dielectric constant of CS layers have a similar effect as band offset on solar cell performance. Our results have obvious implications toward the selection of appropriate materials as CS layers, and hence, are of broad interest to the community.**

***Index Terms*— Efficiency tradeoffs, photovoltaic cells, semiconductor device modeling.**

I. Introduction

SILICON-BASED heterojunction devices with carrier-selective (CS) contacts are increasingly explored as a cost effective alternative for the conventional diffused p-n junction-based c-Silicon solar cells [1]–[12]. Indeed, various techniques such as atomic layer deposition [3], chemical vapor deposition [1], and solution processing [6] are explored for low-temperature fabrication of CS contact layers. Apart from the obvious advantages related to cost effectiveness due to low temperature fabrication processes, large band gap CS layers can also reduce the parasitic absorption at the front end [13]–[16]. As a result, different materials such as a-Si [13], poly Si [17], TiO_2 [1]–[3], LIF_x [4], KF_x [5], PEDOT:PSS [6], MoO_x [7]–[10], V_2O_5 [10], and WO_3 [10] have been extensively studied recently. We note that there have been several modeling [18], [19] efforts as well to understand the device performance of various materials as CS contacts with silicon.

In spite of the above-mentioned exciting research, however, several critical aspects related to Si-based CS solar cells still remain unexplored or not well understood. In this paper, we address the effect of material and interface properties of CS layer on the efficiency of Si-based heterojunction solar cells through detailed analytical (Section II) and numerical modeling (Section III). Then, using the given information, we find out which pair of materials is best suited for Si-based solar cells. Our results indicate that the performance of the solar cell is significantly affected by the band discontinuity between the CS layer and Si (respective bands)—and perfect band alignment is, surprisingly, not a desirable aspect. Furthermore, we provide a detailed map of efficiency versus CS material parameters which could be of immense interest to the community to *a priori* evaluate the performance of any pair of materials as CS layers.

Manuscript received January 24, 2018; revised March 14, 2018; accepted March 23, 2018. Date of publication April 24, 2018; date of current version May 21, 2018. This work was supported in part by the Solar Energy Research Institute for India and the United States, in part by the U.S. Department of Energy under Contract DE-AC36-08GO28308, and in part by the Government of India's Department of Science and Technology under Contract IUSSTF/JCERDC-SERIIUS/2012. The review of this paper was arranged by Editor A. G. Aberle. *(Corresponding authors: Nithin Chatterji, Pradeep R. Nair.)*

N. Chatterji and P. R. Nair are with the Department of Electrical Engineering, IIT Bombay, Mumbai 400076, India (e-mail: nithin@ee.iitb.ac.in; prnair@ee.iitb.ac.in).

A. Antony is with the Department of Energy Science and Engineering, IIT Bombay, Mumbai 400076, India (e-mail: aldrinantony@iitb.ac.in).

Color versions of one or more of the figures in this paper are available online at http://ieeexplore.ieee.org.

Digital Object Identifier 10.1109/TED.2018.2822938

II. Analytical Model

To explore the efficiency tradeoff in Si-based CS solar cells, we first develop an analytical model. Fig. 1 shows the band level alignments of such a solar cell (material parameters are provided in appendix A). Here, ESL and HSL denote the electron- and hole-selective layers, respectively. The parameters that dictate the efficiency of a solar cell are the open-circuit potential (V_{oc}), short-circuit current (J_{sc}), and the fill factor (FF) [20]. Of the above-mentioned parameters, the maximum achievable V_{oc} is dictated by the detailed balance of carrier generation with various recombination processes. Similarly, J_{sc} is a measure of the photogenerated carrier collection efficiency under short-circuit conditions, while FF is more influenced by the collection efficiency at the maximum power point condition. In addition to carrier recombination in bulk Si, interface recombination also critically affects the solar cell performance and as such is influenced by various parameters such as the material properties of the CS layer (which includes the band alignment with c-Si, doping levels, and the complex refractive index), Si/CS layer interface quality (i.e., interface traps and band bending), and the nature of transparent conductive oxide (TCO) contact with the CS layer. In the following, we develop an analytical model to predict the variation of the above-mentioned three performance metrics as a function of various material parameters. The metal or TCO contact with CS layers are assumed as ohmic in this paper (which is valid for heavily doped CS layers or in the presence of significant

interface traps) and the effect of a Schottky contact between the TCO and the CS layer is addressed in Appendix D.

Detailed Balance: For any solar cell, under steady-state conditions, the following detailed balance relation is always valid:

$$\int G dx = -\frac{J}{q} + R_{\text{bulk}} + R_{\text{interface}} \tag{1}$$

where the left integral is the net carrier generation rate, the first term on the right-hand side (RHS) is the current through the solar cell, the second term in the RHS is the net recombination in the bulk of the semiconductor while the last term on the RHS indicates the recombination at any material interfaces. The interface recombination component is given as [21]

$$R_{\text{interface}} = \int_{E_v}^{E_c} \frac{n_s p_s - n_i^2}{\frac{n_s + n_{1s}}{c_{ps}} + \frac{p_s + p_{1s}}{c_{ns}}} D_{\text{it}}\, dE \tag{2}$$

where n_s, p_s, and D_{it} denote the electron density, the hole density, and the trap density at the material interface, while c_{ps} and c_{ns} are the surface electron and hole capture coefficients, respectively. We note that interface recombination should be accounted for all CS/Si interfaces in (1), although only one such interface is explicitly mentioned in (2). We will now use (1) and (2) to predict the performance of Si-based heterojunction solar cells, as detailed in the following.

A. Open-Circuit Voltage V_{oc}

Under V_{oc} conditions, we have $J = 0$ in (1). Accordingly, the separation between the quasi-Fermi levels indicates that [20] $V_{\text{oc}} = F_n - F_p = (kT/q)\ln(np/n_i^2)$. Furthermore, assuming low-level injection conditions, the bulk majority carrier density is $p = N_A$, the Si doping. And, the bulk minority carrier electron density is $n_b = (n_i^2/N_A)e^{qV_{\text{oc}}/kT}$. Under such conditions, the bulk recombination can be approximated as $R_{\text{bulk}} \sim (n_b/\tau_b)w_{\text{Si}}$, where τ_b is the bulk lifetime which includes the Shockley–Read–Hall (SRH), radiative recombination, and Auger recombination mechanisms, and w_{Si} is the silicon substrate thickness. Accordingly, for low levels of illumination, we have $1/\tau_b = 1/\tau_{\text{SRH}} + BN_A + CN_A^2$, where B is the radiative recombination coefficient and C is the Auger recombination coefficient.

The interface recombination can be evaluated in a compact form using (2). As the quasi-Fermi levels remain spatially constant at V_{oc}, the interface carrier densities are given as

$$p_s = N_A\, e^{-\frac{q\psi_{\text{Si}}}{kT}} \tag{3}$$

$$n_s = \frac{n_i^2}{N_A} e^{\frac{qV_{\text{oc}}}{kT}}\, e^{+\frac{q\psi_{\text{Si}}}{kT}} \tag{4}$$

where p_s and n_s are the hole and the electron densities, respectively, at the CS/c-Si interface and ψ_{Si} is the band bending in c-Si.

Equations (1) and (2) allow us to estimate the asymptotic limits of V_{oc}. For example, in the absence of any interface recombination and uniform carrier generation rate G, the maximum achievable V_{oc} for a solar cell is given as

$$V_{\text{oc,max}} = \frac{kT}{q}\ln\left(\frac{G\tau_b N_A}{n_i^2}\right). \tag{5}$$

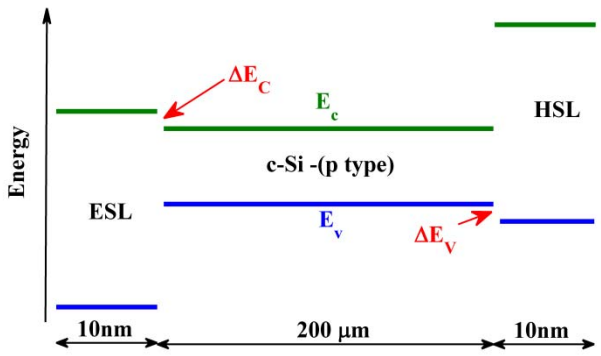

Fig. 1. Energy level alignments of a Si-based carrier selective solar cell. Refer Appendix A for simulation parameters.

On the other hand, the presence of interface recombination reduces the achievable V_{oc} from this limit. An asymptotic limit for the minimum achievable V_{oc} can be obtained using $Gw_{\text{Si}} = R_{\text{interface}}$ [see (1)]. However, the maximum $R_{\text{interface}}$ happens under the conditions $p_s = n_s$ [under the assumption $c_{ps} = c_{ns}$, see (2)]. Under such conditions, (3) and (4) indicate that

$$\psi_{\text{Si,min}} = \psi_F - \frac{V_{\text{OC,min}}}{2} \tag{6}$$

where $\psi_F = (kT/q)\ln(N_A/n_i)$. Accordingly, for uniform D_{it}, the minimum achievable V_{oc} is given as

$$V_{\text{oc,min}} = \frac{2kT}{q}\ln\left(\frac{2Gw_{\text{Si}}}{c_{\text{ns}} D_{\text{it}} E_{g,\text{Si}} n_i}\right). \tag{7}$$

Here, $E_{g,\text{Si}}$ is the bandgap of c-Si. Equations (5) and (6) predict the upper and lower bounds for V_{oc} that could be achieved by any CS solar cell (note that we have considered recombination at ESL/Si layer only, but the model could be easily extended to account for recombination at HSL/Si interface as well). For typical values of 1 sun illumination with $\tau_{\text{SRH}} = 1$ ms, $B = 1.1 \times^{-14}$ cm$^3 \cdot$ s^{-1}, and $C_{(n,p)} \approx 10^{-31}$ cm$^6 \cdot$ s^{-1}, we get $V_{\text{oc,max}} = 750$ mV, while $V_{\text{oc,min}} = 560$ mV.

The asymptotic limit for the theoretical minimum V_{oc} for any D_{it}, provided by (7), could be made more accurate to account for the bulk recombination as follows. The detailed balance [(1)] under V_{oc} conditions along with (6) leads to

$$\frac{n_i^2 w_{\text{Si}}}{N_A \tau_b} e^{\frac{qV_{\text{oc,min}}}{kT}} + \frac{n_i^2 c_{ns} D_{\text{it}} E_{g,\text{Si}}}{2N_A} e^{\frac{q\psi_F}{kT}} e^{\frac{qV_{\text{oc,min}}}{2kT}} - Gw_{\text{Si}} = 0. \tag{8}$$

Fig. 2(a) shows the variation of $V_{\text{oc,min}}$ as a function of D_{it}. The symbols represent solution of (8), while the solid lines are solutions of the asymptotic limits given by (5) and (7). For low D_{it}, $V_{\text{oc,min}}$ is well predicted by (5) while for large D_{it}, (7) predicts the trends.

It is interesting to note that $V_{\text{oc,min}}$ depends only on the interface quality (i.e., D_{it}) and is independent of ESL parameters. However, this is subject to the condition $n_s = p_s$ which might be satisfied for only certain unique combinations of other material parameters. To explore this further, we note that the device electrostatics indicate that V_{oc} is related to the

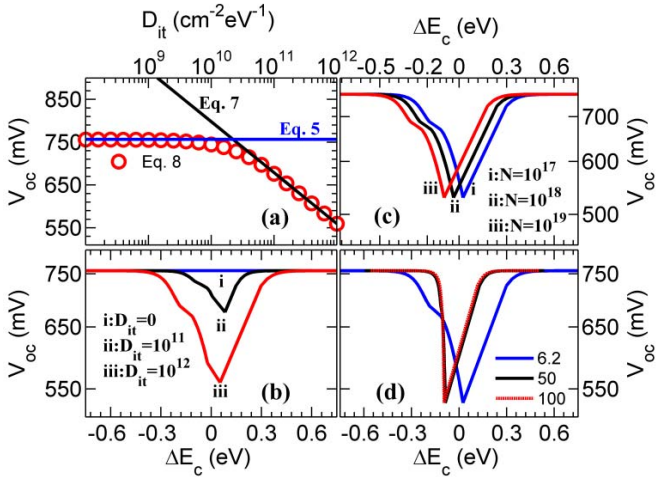

Fig. 2. Model predictions for V_{oc}. (a) Minimum V_{oc} as a function of D_{it}($cm^{-2} \cdot eV^{-1}$). (b) V_{oc} as a function of ΔE_c. (c) Effect of doping density variation $N_{D,ESL}$(cm^{-3}). (d) Effect of dielectric constant ε_{ESL} (mentioned as legends).

other material parameters by the relation

$$V_{oc} = V_{bi} - \psi_{Si} - \psi_{ESL} \tag{9}$$

where the built-in potential $V_{bi} = \text{abs}(\varphi_{ESL} - \varphi_{Si})$, the difference in the work function of c-Si and ESL, and ψ_{ESL} is the potential drop in ESL under V_{oc} conditions (estimated in Appendix B). Equation (9) allows us to estimate the conditions at which a solar cell could achieve $V_{oc,min}$ as predicted by (7). For this the first-order estimate is needed for ψ_{ESL}, which is provided in Appendix B, and

$$V_{bi} = \Delta E_c + \frac{E_{g,Si} - E_{g,ESL}}{2} + \frac{kT}{q}\ln\left(\frac{N_A}{ni}\frac{N_{D,ESL}}{n_{i,ESL}}\right). \tag{10}$$

where ΔE_c = EA(Si) − EA(ESL) is the difference in electron affinities, $E_{g,ESL}$ is the bandgap of ESL, and $n_{i,ESL}$ and $N_{D,ESL}$ are the intrinsic and doping concentrations in ESL, respectively. It is now evident from (6)–(10) that there exists a particular combination of various parameters such as ΔE_c, dielectric constant, and doping density, at which $V_{oc,min}$ is achieved for a particular D_{it}. Any deviation in any of these parameters would result in V_{oc} larger than $V_{oc,min}$ (for that particular D_{it}). Indeed, with appropriate parameters, (9) indicates that band alignment for the minimum V_{oc} conditions is $\Delta E_c \sim 50$ meV for D_{it} in the range of $10^{10} - 10^{12}$ $cm^{-2} \cdot eV^{-1}$. Accordingly, this model predicts that for large ΔE_c, V_{oc} should improve significantly and approach $V_{oc,max}$ asymptotically—a hypothesis which could be tested against detailed numerical simulations.

We now explore the dependence of V_{oc} on CS layer material parameters such as ΔE_c, D_{it}, doping density, and dielectric constant of the CS layer. As discussed earlier, V_{oc} of a device could be different from that predicted by (7) and (8), as the resultant band bending might not ensure the condition $n_s = p_s$ at the interface. An analytical model to address this general case (i.e.,V_{oc} under the conditions $n_s \neq p_s$) is described in Appendix C. The results from the analytical model are plotted in Fig. 2(b)–(d). Fig. 2(b) shows the variation of V_{oc} as a function of ΔE_c. Interestingly, Fig. 2(b) shows that V_{oc} is limited by the bulk lifetime if $D_{it} = 0$ and is predicted by (5). For nonzero D_{it}, V_{oc} is minimum for small ΔE_c and is given by (7). Equation (10) indicates that an increase in ΔE_c leads to an increase in V_{bi}, which leads to an increase in ψ_{Si} [see (9)]. Accordingly, one type of carrier dominates the other near the interface [see (3) and (4)] which results in reduced interface recombination, hence better V_{oc}. Hence, for large ΔE_c, V_{oc} approaches the asymptotic limit predicted by (5). Furthermore, Fig. 2(c) shows the effect of doping in ESL ($N_{D,ESL}$) on V_{oc} in the presence of $D_{it} = 10^{12}$ $cm^{-2} \cdot eV^{-1}$. This trend is also well predicted by the analytical model. An increase in $N_{D,ESL}$ tends to increase V_{bi} [see (10)], and hence, $V_{oc,min}$ condition will be met with a reduction in ΔE_c. As a result, the curve shifts to the left with an increase in $N_{D,ESL}$ [Fig. 2(c)]. Fig. 2(d) shows the effect of dielectric constant (ε_{ESL}) in ESL in the presence of $D_{it} = 10^{12}$ $cm^{-2} \cdot eV^{-1}$. An increase in ε_{ESL} results in a reduction of ψ_{ESL} (see Appendix B) and the $V_{oc,min}$ conditions will be met with a decrease in ΔE_c [see (9) and (10)]. Accordingly, the curve shifts to the left as well.

B. J_{sc} and FF

The analytical results in Section II-A indicate that there should be a minimum band offset of around 0.2–0.4 eV for optimal V_{oc}. However, this analysis still does not predict the trends for efficiency unless accounted for J_{sc} and FF—both depend on the collection efficiency of carriers at respective electrodes. Under short-circuit conditions, $R_{interface}$ is negligible (as $n_s p_s \sim n_i^2$), and $n_s \sim (n_i^2/N_A)e^{+q\psi_{Si}/kT}$. Note that photocurrent collected through the ESL, which is J_{sc}, is now given as

$$J_{sc} \propto n_s e^{-\frac{\Delta E_c}{kT}} \tag{11}$$

where n_s on the RHS denotes the supply of electrons and $e^{-\Delta E_c/kT}$ denotes the probability of crossing the barrier (i.e., for $\Delta E_c > 0$. Otherwise, the current will be limited by the diffusion of electrons from bulk to Si/ESL interface). An equivalent expression for (9) under short-circuit conditions indicates that $V_{bi} - \psi_{Si} - \psi_{ESL} = 0$, where V_{bi} is still given by (10). As such, an increase in ΔE_c will result in an increase in both V_{bi} and ψ_{Si}, and hence, the supply n_s increases exponentially with ΔE_c while the over-the-barrier transport probability decreases exponentially with ΔE_c. Accordingly, (11) predicts that J_{sc} is invariant with ΔE_c and this invariance is expected till the Si surface becomes strongly inverted. Once the surface becomes strongly inverted, n_s will not increase appreciably any further. However, the over-the-barrier transport probability will still decrease exponentially with ΔE_c, thus, leading to a decrease in J_{sc}. Based on this argument, we expect J_{sc} to remain invariant till a particular ΔE_c is obtained (which is ~0.4 eV as shown by numerical simulations in subsequent sections).

The variation of FF with ΔE_c is rather difficult to anticipate. For small ΔE_c, we expect that the FF might follow the trends of V_{oc} as predicted by the analytical relationship between FF and V_{oc} [22]. For large ΔE_c, the FF decreases due

to the reduction in collection efficiency of photogenerated carriers (trends similar to the short-circuit conditions).

The analysis in this section predicts that the performance of a CS solar cell is not at its optimal value for perfect band alignment—indeed, the best device performance could be at an optimal ΔE_c, which in turn could depend on the interface recombination as well. The same model predicts that the performance improves with an increase in the doping density and dielectric constant of the CS material.

III. Numerical Simulations

To further explore the predictions from the analytical model, we performed detailed numerical simulations (self-consistent solution of Poisson and drift diffusion equations) [23]. Appendix A provides the list of parameters used in simulations. The effect of band discontinuity between c-Si and ESL in the presence and absence of traps is explored using numerical simulations. For this, we first study the effect of conduction band offset ΔE_c at the ESL/Si interface while keeping $\Delta E_v = 0$ eV for HSL. Uniform density of interface traps was assumed at the ESL/c-Si interface. Later, the effect of band offsets at Si/HSL interface is also discussed.

Fig. 3(a) and (b) shows the energy band diagram near the ESL under short-circuit conditions for $\Delta E_c = 0$ eV and $\Delta E_c = 0.4$ eV, respectively. It is evident that the band bending in c-Si is more in the case for $\Delta E_c = 0.4$ eV. This large band bending creates an inversion region near the c-Si/ESL interface. Fig. 3(c) and (d) shows the variation in the carrier densities with bias at the ESL/c-Si interface in the c-Si edge for $\Delta E_c = 0$ eV and $\Delta E_c = 0.4$ eV, respectively. The minority carrier density, which dictates the rate of trap-assisted recombination, is significantly lower for the case with large ΔE_c. [Fig. 3(e) and (f) shows a comparison of the net recombination rates.] As a result, V_{oc} is expected to increase with ΔE_c, similar to that of field effect passivation [24] and efficiency improvement due to inversion [25], [26]. We expect similar effect for negative ΔE_c as well. Negative ΔE_c leads to an increase in p_s and reduction in n_s which reduces the interface recombination term [see (12) in Appendix B]. This reduction in recombination leads to an improvement in V_{oc} with negative ΔE_c.

The above-mentioned insights are well supported by the trends related to dark IV characteristics as well. For example, the effect of ΔE_c on the dark IV characteristics in the presence of interface trap density of 10^{12} cm^{-2}·eV^{-1} is shown in Fig. 4. Ideality factor is close to 2 at $\Delta E_c = 0$ eVwhich corresponds to significant recombination due to the interface traps. Ideality factor decreases with ΔE_c and reaches a value close to 1 near $\Delta E_c = \pm 0.4$ eV. This indicates a reduction in the detrimental effect of interface traps at larger values of ΔE_c as discussed earlier. Note that J_0 follows the trend of the ideality factor. J_0 has the maximum value at $\Delta E_c = 0$ eV as a result of significant interface recombination—which is also confirmed by carrier densities, n_s and p_s in Fig. 3.

Fig. 5 shows the effect of discontinuity in the conduction band between ESL and c-Si on the solar cell performance. Fig. 5(a) shows the variation of V_{oc} with ΔE_c. The results

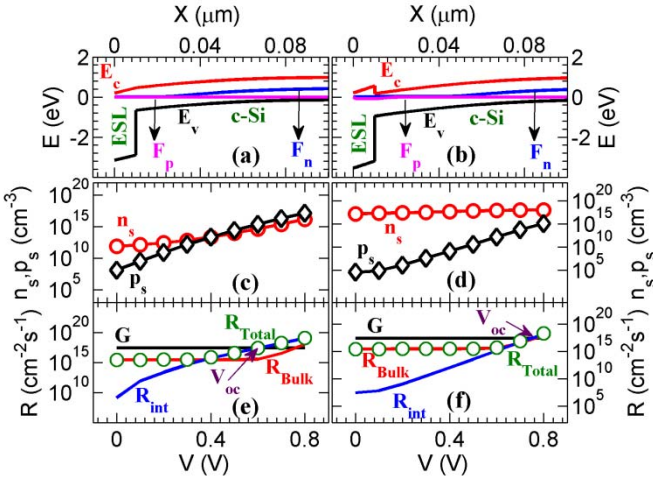

Fig. 3. Effect of ΔE_c on band bending and carrier densities at c-Si/ESL interface with $D_{it} = 10^{12}$ cm^{-2} · eV^{-1} (numerical simulations, under illumination). (a) and (b) Energy band diagram for $\Delta E_c = 0$ eV and $\Delta E_c = 0.4$ eV, respectively, at short-circuit conditions. (c) and (d) Variation in interface carrier densities n_s and p_s with bias. (e) and (f) Variation of recombination and generation rates with bias for $\Delta E_c = 0$ eV and $\Delta E_c = 0.4$ eV, respectively. G, R_{Bulk}, $R_{interface}$, and R_{Total} (symbols) represent the generation rate, bulk recombination rate, interface recombination rate, and total recombination rate of the electrons in the device. V_{oc} is the point of intersection of the generation rate and total recombination.

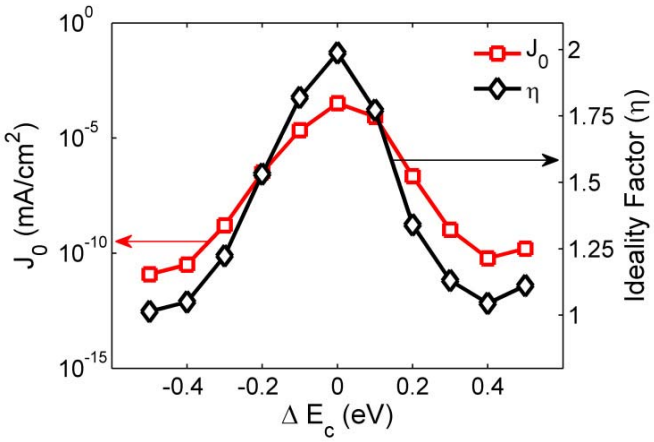

Fig. 4. Effect of ΔE_c on J_0 and ideality factor in the dark IV with interface traps ($D_{it} = 10^{12}$cm^{-2} · eV^{-1}). This indicates that J_0 and ideality factor improve as the band offset varies from $\Delta E_c = 0$ eV conditions due to the reduction in interface recombination.

are similar to the analytical predictions in Fig. 2(b). In the presence of traps, the variation in V_{oc} is almost symmetric with ΔE_c. The minimum value of V_{oc} is at $\Delta E_c \sim 0$ eV and it increases as ΔE_c increases (i.e., the magnitude), as already explained.

Variation of J_{sc} with ΔE_c is shown in Fig. 5(b). As seen in the analytical model, J_{sc} is not affected till a particular value of ΔE_c is reached. After that, the over-the-barrier transport of carriers to ESL decreases with an increase in ΔE_c. The collection of electrons is not typically affected with negative ΔE_c, as the band bending under short-circuit conditions is large enough [Fig. 3(a) and (b)], and hence, there is no effect of interface traps on J_{sc} for negative ΔE_c.

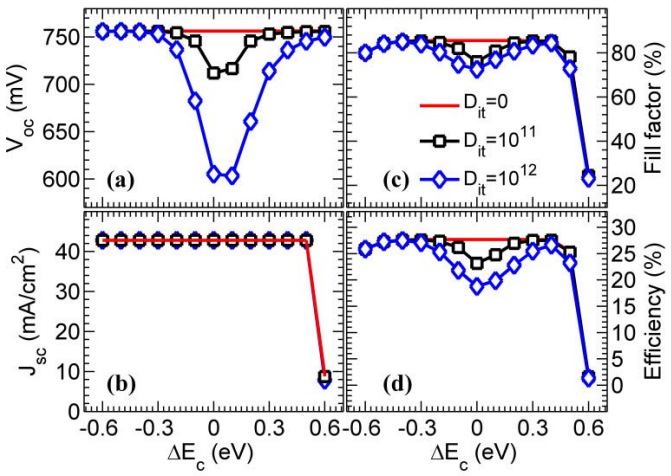

Fig. 5. Effect of ΔE_C on performance parameters. (a) V_{oc}, (b) J_{sc}, (c) FF, and (d) efficiency of CS Si solar cells for different D_{it}(cm$^{-2}\cdot$eV^{-1}) values. Note that the trends are broadly consistent with the analytical model and indicate that surprisingly, the solar cell performance is ideal for a nonzero band offset.

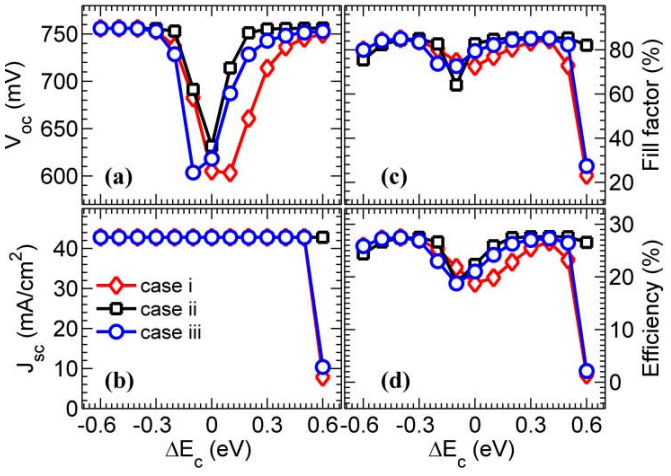

Fig. 6. Effect of doping and dielectric constant in ESL on solar cell performance parameters. (a) V_{oc}, (b) J_{sc}, (c) FF, and (d) efficiency for $D_{it} = 10^{12}$ cm$^{-2}\cdot$eV^{-1}. Case (i) has an ESL doping of 10^{17} cm^{-3} and dielectric constant of 6.2, case (ii) has an ESL doping of 10^{17} cm^{-3} and dielectric constant of 85, and case (iii) has an ESL doping of 10^{18} cm^{-3} and dielectric constant of 6.2. The results indicate that the passivation quality increases with doping and dielectric constant for the same positive value of ΔE_C.

Fig. 5(c) shows the variation in FF with ΔE_c. Without any interface traps, FF is not affected till $\Delta E_c = 0.4$ eV. Beyond $\Delta E_c = 0.4$ eV, over-the-barrier transport of electrons from c-Si to ESL is affected under the maximum power point conditions, and hence, gets reflected in FF. The results show that the presence of interface traps significantly affects the FF for lower values of ΔE_c [also see Fig. 3(e)]. Specifically, under such conditions, the FF follows the V_{oc} trends for both the negative and positive values of ΔE_c, as predicted by the empirical relationship connecting FF with V_{oc} [22].

Finally, the solar cell efficiency [see Fig. 5(d)] also follows the trends of V_{oc} and has its minimum at perfect band alignment conditions. The performance improves in both the directions, till over-the-barrier transport is affected and the efficiency becomes limited by FF and J_{sc}. Accordingly, the best device performance is observed at $\Delta E_c \approx 0.3$–0.4 eV.

A. Effect of Doping and Dielectric Constant in the SL

Fig. 6 shows the effect of doping and dielectric in ESL with ΔE_c on the solar cell performance parameters. Fig. 6(a) shows the variation of V_{oc} with ΔE_c. It shows that the curve shits to the left with an increase in both the doping and the dielectric constant in ESL. As explained in Section II, this is due to the increase in band bending in the c-Si region near ESL with an increase in both doping and dielectric constant.

B. Effect of Band Discontinuity Between HSL and c-Si

Fig. 7 shows the effect of ΔE_V between c-Si and HSL in the presence of interface traps on solar cell performance parameters. As before, here we assume ideal conditions at ESL/c-Si interface (i.e., zero band offset and no traps). Fig. 7(a) and (b) shows the variation of V_{oc} and J_{sc}, respectively, with ΔE_V. While the change in V_{oc} is very similar to that observed with ESL/c-Si band offset (see Section III-A), surprisingly, there are significant differences in the J_{sc} trends. We observe that

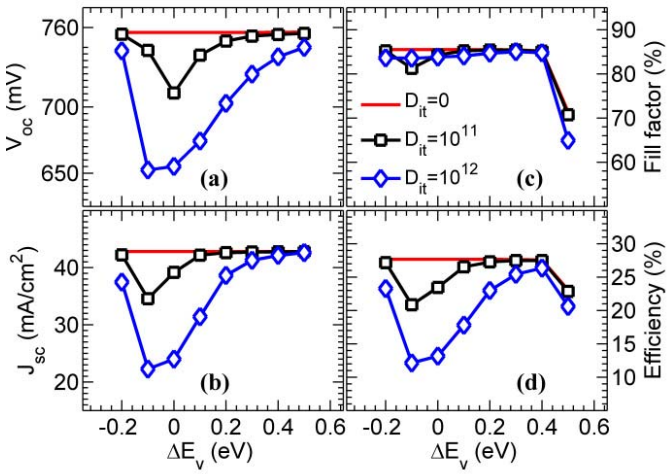

Fig. 7. Effect of ΔE_V at Si/HSL interface on the performance parameters. (a) V_{oc}, (b) J_{sc}, (c) FF, and (d) efficiency of CS Si solar cells for different D_{it} (cm$^{-2}\cdot$eV^{-1}) values. Here both V_{oc} and J_{sc} are affected by the change in the passivation quality at the c-Si/HSL interface due to variation in ΔE_V.

J_{sc} varies with ΔE_V in contrast to the trends for ESL/Si interface (see Section III-A). These puzzling trends are due to the distinct nature of ESL/c-Si and c-Si/HSL junctions. While the former is a PN junction, the latter is a PP$^+$ junction. Accordingly, the band bending in c-Si is more at the ESL/c-Si junction than that of the c-Si/HSL junction. This reduction in band bending increases the recombination loss at c-Si/HSL interface which reduces the collection efficiency of holes, hence J_{sc}.

Fig. 7(c) and (d) shows the variation of FF and efficiency, respectively, with ΔE_v. Due to the smaller band bending in c-Si near the HSL, the effect of interface traps is more at the c-Si/HSL interface compared to ESL/c-Si interface, as shown

by the lower values of efficiency for the corresponding values of band discontinuity.

IV. Implications

Our results show that interface engineering is very crucial for Si-based CS solar cells. Indeed, for similar band offsets, the presence of traps is more detrimental at the selective layer that extracts the majority carrier. For example, Figs. 5 and 7 indicate that traps at HSL/c-Si interface (where holes, the majority carriers for p-substrate, are collected) reduce the efficiency quite significantly as compared to the same trap density at ESL/c-Si interface (where electrons, the minority carriers, are collected). Note that similar conclusions will hold good for n-type substrates as well, as the above-mentioned effect is only influenced by the amount of band bending in c-Si. This has interesting implications on the choice of materials for Si-based CS solar cells. While the presence of a p-n junction, and hence, the associated band bending allows considerable freedom in the choice of selective layer to extract the minority carriers, the selective layer for extraction of majority carriers should be chosen carefully with near perfect interface passivation properties. Accordingly, among the various choices, we speculate that a-Si based selective layers might be the most promising to extract the majority carrier (as a-Si could provide excellent interface passivation), while many other materials could be successful to extract the minority carriers.

Finally, our results indicate that parameters such as band discontinuity, doping, and dielectric constant of CS materials are the critical parameters that could affect the interface recombination, and hence, the efficiency of Si-based CS solar cells. This information allows us to compare the promises of various CS materials such as a-Si ($\Delta E_c \sim 0.3$ eV and $\varepsilon = 11.9$) [11], TiO_2 ($\Delta E_c \sim 0.05$ eV and $\varepsilon \sim 85$) [16], and ZnO($\Delta E_c \sim -0.6$eV and $\varepsilon \sim 9$) [27] as ESL. For similar doping and D_{it}, our results indicate that a-Si might be the optimal choice and followed by ZnO. TiO_2 has the drawback of almost perfect band alignment; however, it has the advantage of large dielectric constant. These trends indicate that a-Si based CS contacts would continue to yield the best performance as both the ESL and HSL (see Section III-C also)—a conclusion also partially supported by the excellent efficiencies achieved by HIT solar cells [11]. Future exploration of new CS materials can be immensely benefitted through a quantitative evaluation of material parameters (band offset, doping density, dielectric constant, and interface trap density) as detailed in this paper. We would like to stress that these conclusions/insights are also dependent on the properties of the TCO/ESL contact. The analysis so far provided in this paper relied on the assumption of ohmic conditions at TCO/CS contact. At the other extreme, one could have significant Schottky barrier effects at the TCO/CS contact. Indeed our results (Appendix D) indicate that non-ohmic nature of TCO/ESL contact (Schottky junction, Fermi-level pinning, etc.), and so on) affect the performance in a nontrivial manner—which could be significantly different from that of the other asymptotic limit of ohmic contacts. Even then, this paper serves as a benchmark that the functional dependence of critical parameters is clearly elucidated and any deviation observed could then be subsequently explored in a coherent and systematic way. Given the trends toward low-temperature processing, it is evident that the future studies in this regard should account for both the effect of TCO work function and trap-assisted tunneling at TCO/CS contact.

V. Conclusions

To summarize, here, we addressed the effect of CS material properties on the solar cell performance. We developed an analytical model to evaluate the effect of CS material parameters on the efficiency and the same was validated using detailed numerical simulations. Curiously, we find that the optimal band alignment depends on the interface quality. If the interface quality is very good, then the efficiency is limited by over-the-barrier transport of carriers, and hence, small band offsets do not affect the performance. Otherwise, for not so ideal conditions at the interface, a band offset of around 0.2–0.4 eV provides sufficient band bending to reduce the effect of interface recombination, thus improving the performance. In addition, our results show that the need for excellent interface passivation is more at the majority carrier extraction layer than at the minority carrier extraction layer. Furthermore, we find that both the doping and the dielectric constant of the CS material have a similar effect on the performance, and the TCO/CS contact properties could significantly influence the results. Hence, we suggest that the future work in this regard should address a broader range of TCO work function along with trap-assisted tunneling at TCO/CS interface. These interesting insights could be of broad interest to the community toward the selection of appropriate materials as CS layers.

Appendix A
Parameters Used in Simulations

To study the band offset effects, ΔE_c at the ESL/c-Si interface is varied from -0.6 to $+0.6$eV, while the barrier for holes is kept fixed (2.28 eV). At the c-Si/HSL interface, ΔE_v is varied from -0.2 to $+0.5$ eV, while the barrier for electrons is kept fixed (2.28 eV). As a result, the band gap (and also the electron affinity) of ESL varies with the corresponding band offset used in each simulation. Accordingly, in our simulations the ESL band gap varies from 2.8 to 4 eV, which is comparable to the band gap of TiO_2 ($\sim$3.4 eV). Similar arguments hold good for HSL as well. For ease of analysis, we have used the same dielectric constant (6.2) for both ESL and HSL. However, many materials could have large dielectric constants (like TiO_2), and the effect of large dielectric constant was explored by both the analytical modeling and numerical simulations (also mentioned in Section IV). We considered uniform distribution of traps at the interface of CS layer and Si. The capture cross section of these traps was assumed as 10^{-16} cm^{-2}. The radiative recombination coefficient in c-Si is assumed as 1.1×10^{-14} cm$^3 \cdot$ s^{-1} [28]. The Auger coefficient for electrons and holes in c-Si is assumed as 1×10^{-31} cm$^6\cdot$s^{-1} and 0.79×10^{-31} cm$^6\cdot$s^{-1} [29], respectively. The remaining parameters are provided in Table I.

TABLE I
PARAMETERS USED IN NUMERICAL SIMULATIONS

Parameter	c-Si	ESL	HSL
N_c, N_v (10^{19}cm^{-3})	3.23, 1.83	25, 25	25, 25
Mobility((n, p) $cm^2V^{-1}s^{-1}$)	1417, 470.5	20, 2	20, 2
τ SRH (s)	10^{-3}	10^{-6}	10^{-6}
Doping(cm^{-3})n/p	p - 10^{17}	n - 10^{17}	p - 10^{17}

APPENDIX B
ANALYTICAL MODEL FOR ψ_{ESL}

A first-order estimate for the potential drop in ESL can be given as

$$\psi_{\rm ESL} \sim (Q_i + Q_{\rm bulk}) w_{\rm ESL}/\varepsilon_{\rm ESL} \tag{12}$$

where Q_i is the net charge due to the interface states ($Q_i = -qD_{\rm it}(E_{Fn} - E_i) + qD_{\rm it}(E_i - E_{Fp})$ [21], and the depletion charge in Si is $Q_{\rm bulk} = -\sqrt{2\varepsilon_{Si} q N_A \psi_{\rm Si}}$($\varepsilon_{\rm Si}$ and $\varepsilon_{\rm ESL}$ are the dielectric constant in c-Si and ESL, respectively).

APPENDIX C
ANALYTICAL MODEL FOR V_{OC}

Equations (3) and (4) indicate that the majority carriers at the interface could be either electrons or holes (which will be influenced by the parameters $V_{\rm oc}$ and $\psi_{\rm Si}$). Accordingly, we obtain different relations for tradeoff of $V_{\rm oc}$ versus carrier densities, as follows. Specifically, evaluating $R_{\rm interface}$ using (2) under the assumption of $p_s \gg n_s$ and uniform $D_{\rm it}$, with $R_{\rm bulk}$ as evaluated in Section II-A, (1) can be approximated as

$$Gw \approx \frac{n_i^2}{N_A} e^{\frac{qV_{\rm oc}}{kT}} \left(\frac{w_{\rm Si}}{\tau_b} + c_{\rm ns} D_{\rm it} e^{+\frac{q V_{\rm Si}}{kT}} E_{g,\rm si} \right) \tag{13}$$

where $E_{g,\rm si}$ is the bandgap of c-Si [Note that (13) represents interface recombination at only one interface, say ESL/Si. However, it could be easily extended to consider recombination at multiple interfaces.] On the other hand, the same procedure with $n_s \gg p_s$ leads to

$$Gw \approx \frac{n_i^2}{N_A} e^{\frac{qV_{\rm oc}}{kT}} \frac{w_{Si}}{\tau_{\rm bulk}} + c_{ps} D_{it} N_A e^{-\frac{q\psi_{\rm Si}}{kT}} E_{g,\rm si}. \tag{14}$$

$V_{\rm oc}$ can be estimated for different values of $\psi_{\rm Si}$ using (13) for $p_s > n_s$ and (14) for $n_s > p_s$. However, $\psi_{\rm Si}$ under $V_{\rm oc}$ conditions is still an unknown factor and it can be related to various parameters of interest such as the band offset and doping of ESL. Now, (9), (10), (13) and (14) can be self-consistently solved to evaluate the $V_{\rm oc}$ tradeoff with various material parameters associated with Si-based CS solar cells and the results of which are plotted in Fig. 2.

APPENDIX D
EFFECT OF TCO CONTACT WITH ESL

The results in this paper relied on the assumption that the TCO/ESL contact is ohmic in nature—which is expected in the presence of heavy doping of ESL and/or in the presence of significant trap-assisted tunneling of electrons from ESL to TCO. (There could be issues related to Fermi-level pinning as well [18].) However, in the view of the above-mentioned issue, TCO/ESL Schottky junction might be of concern for Si-based CS solar cells, and here, we consider the same. Fig. 8 shows the effect of a Schottky contact of work function 4.7, which corresponds to Indium Tin Oxide (ITO) [30] at ESL on performance parameters with ΔE_c. The results indicate that the nature of TCO/ESL junction can significantly affect the CSC performance. Specifically, Fig. 8(a) shows that negative values of ΔE_c give the best value of $V_{\rm oc}$. Fig. 8(b)–(c) show that $J_{\rm sc}$, FF decreases for positive values of ΔE_c, similar to $V_{\rm oc}$ trends. Finally Fig. 8(d) shows that efficiency, which is the product of $J_{\rm sc}$, FF and $V_{\rm oc}$, varies similarly with ΔE_c.

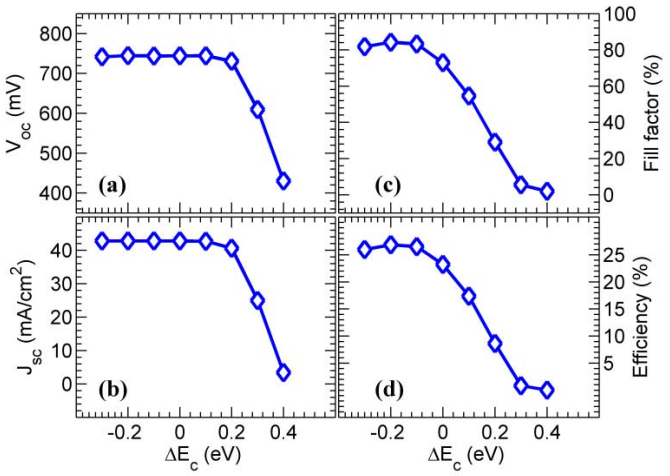

Fig. 8. Effect of ΔE_c with a Schottky contact of work function 4.7 eV at ESL on performance parameters. (a) $V_{\rm oc}$, (b) $J_{\rm sc}$, (c) FF, and (d) efficiency of CS Si solar cells for $D_{\rm it} = 10^{12}$cm^{-2}·eV^{-1}. For this configuration, an optimal value of negative ΔE_c between ESL/c-Si interface gives the best performance.

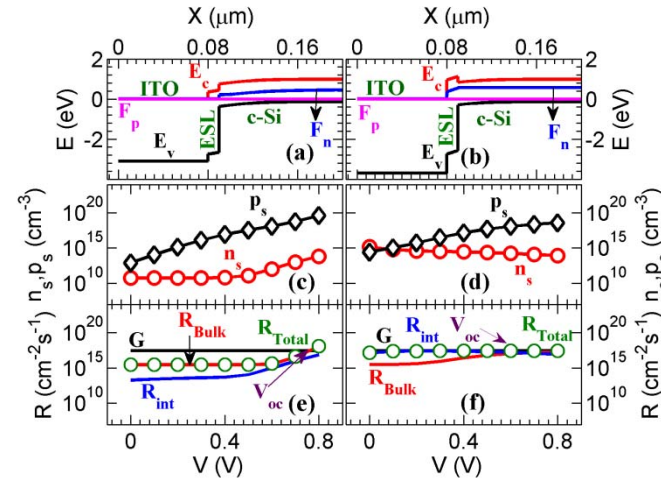

Fig. 9. Effect of ΔE_c on band bending and carrier densities at c-Si/ESL interface with $D_{\rm it} = 10^{12}$ cm^{-2} · eV^{-1}, when a TCO with work function 4.7 is considered as the contact (numerical simulations, under illumination). (a) and (b) Energy band diagram for $\Delta E_c = -0.3$ eV and $\Delta E_c = 0.3$ eV, respectively, at short circuit conditions. (c) and (d) Variation in interface carrier densities n_s and p_s with bias for $\Delta E_c = -0.3$ eV and $\Delta E_c = 0.3$ eV, respectively. (e) and (f) Variation of recombination and generation rates with bias for $\Delta E_c = -0.3$ eV and $\Delta E_c = 0.3$ eV, respectively. The various parameters listed are already defined in Fig. 3.

Insights on the above-mentioned efficiency tradeoff can be obtained from Fig. 9. Fig. 9(a) and (b) shows the energy band diagram near the ESL at short-circuit conditions for $\Delta E_c = -0.3$ eV and $\Delta E_c = 0.3$ eV, respectively. It is evident that the band bending in c-Si is less for both cases compared to the case with the ohmic contact (refer Fig. 3). Fig. 9(c) and (d) shows the variation in the carrier densities with bias at the ESL/c-Si interface in the c-Si edge for $\Delta E_c = -0.3$ eV and $\Delta E_c = 0.3$ eV, respectively. Fig. 9(e) and (f) shows the variation in the generation and recombination rates with bias for $\Delta E_c = -0.3$ eV and $\Delta E_c = 0.3$ eV, respectively. It shows that for $\Delta E_c = -0.3$ eV, bulk recombination is more than interface recombination. However, for $\Delta E_c = 0.3$ eV, the interface recombination term is comparable to the generation rate throughout the voltage range and reduces both J_{sc} as well as V_{oc}.

Acknowledgment

The authors would like to thank the Center of Excellence in Nanoelectronics and the National Center for Photovoltaic Research and Education, IIT Bombay, Mumbai, India, for computational facilities. The authors would like to acknowledge Prof B. M. Arora, Prof. K. L. Narasimhan, and Prof. J. M. Vasi, Department of Electrical Engineering, IIT Bombay, for helpful discussions.

References

[1] S. Avasthi, W. E. McClain, G. Man, A. Kahn, J. Schwartz, and J. C. Sturm, "Hole-blocking titanium-oxide/silicon heterojunction and its application to photovoltaics," *Appl. Phys. Lett.*, vol. 102, no. 20, p. 203901, May 2013.

[2] K. A. Nagamatsu *et al.*, "Titanium dioxide/silicon hole-blocking selective contact to enable double-heterojunction crystalline silicon-based solar cell," *Appl. Phys. Lett.*, vol. 106, no. 12, p. 123906, Mar. 2015.

[3] T. G. Allen *et al.*, "A low resistance calcium/reduced titania passivated contact for high efficiency crystalline silicon solar cells," *Adv. Energy Mater.*, vol. 7, no. 12, p. 1602606, Jun. 2017.

[4] J. Bullock *et al.*, "Lithium fluoride based electron contacts for high efficiency n-type crystalline silicon solar cells," *Adv. Energy Mater.*, vol. 6, no. 14, p. 1600241, Jul. 2016.

[5] J. Bullock *et al.*, "Efficient silicon solar cells with dopant-free asymmetric heterocontacts," *Nat. Energy*, vol. 1, Jan. 2016, Art. no. 15031.

[6] D. Zielke, A. Pazidis, F. Werner, and J. Schmidt, "Organic-Silicon heterojunction solar cells on n-type silicon wafers: The BackPEDOT concept," *Sol. Energy Mater. Sol. Cells*, vol. 131, pp. 110–116, Dec. 2014.

[7] B. Macco, M. F. J. Vos, N. F. W. Thissen, A. A. Bol, and W. M. M. Kessels, "Low-temperature atomic layer deposition of MoOx for silicon heterojunction solar cells," *Phys. Status Solidi-Rapid Res. Lett.*, vol. 9, no. 7, pp. 393–396, Jul. 2015.

[8] M. Bivour, J. Temmler, H. Steinkemper, and M. Hermle, "Molybdenum and tungsten oxide: High work function wide band gap contact materials for hole selective contacts of silicon solar cells," *Sol. Energy Mater. Sol. Cells*, vol. 142, pp. 34–41, Nov. 2015.

[9] J. Geissbühler *et al.*, "22.5% efficient silicon heterojunction solar cell with molybdenum oxide hole collector," *Appl. Phys. Lett.*, vol. 107, no. 8, p. 81601, Aug. 2015.

[10] L. G. Gerling *et al.*, "Transition metal oxides as hole-selective contacts in silicon heterojunctions solar cells," *Sol. Energy Mater. Sol. Cells*, vol. 145, pp. 109–115, Feb. 2016.

[11] K. Masuko *et al.*, "Achievement of more than 25% conversion efficiency with crystalline silicon heterojunction solar cell," *IEEE J. Photovolt.*, vol. 4, no. 6, pp. 1433–1435, Nov. 2014.

[12] F. Feldmann, M. Bivour, C. Reichel, M. Hermle, and S. W. Glunz, "Passivated rear contacts for high-efficiency n-type Si solar cells providing high interface passivation quality and excellent transport characteristics," *Sol. Energy Mater. Sol. Cells*, vol. 120, pp. 270–274, Jan. 2014.

[13] S. de Wolf, A. Descoeudres, Z. C. Holman, and C. Ballif, "High-efficiency silicon heterojunction solar cells: A review," *Green*, vol. 2, no. 1, pp. 7–24, Mar. 2012.

[14] Z. C. Holman *et al.*, "Current losses at the front of silicon heterojunction solar cells," *IEEE J. Photovolt.*, vol. 2, no. 1, pp. 7–15, Jan. 2012.

[15] H. Fujiwara and M. Kondo, "Effects of *a*-i: H layer thicknesses on the performance of *a*-Si: H/*c*-Si heterojunction solar cells," *J. Appl. Phys.*, vol. 101, no. 5, p. 054516, Mar. 2007.

[16] S. M. de Nicolás, D. Muñoz, A. S. Ozanne, N. Nguyen, and P. J. Ribeyron, "Optimisation of doped amorphous silicon layers applied to heterojunction solar cells," *Energy Procedia*, vol. 8, pp. 226–231, Apr. 2011.

[17] B. Nemeth *et al.*, "Polycrystalline silicon passivated tunneling contacts for high efficiency silicon solar cells," *J. Mater. Res.*, vol. 31, no. 6, pp. 671–681, Mar. 2016.

[18] R. Islam, K. N. Nazif, and K. C. Saraswat, "Si heterojunction solar cells: A simulation study of the design issues," *IEEE Trans. Electron Devices*, vol. 63, no. 12, pp. 4788–4795, Dec. 2016.

[19] H. Imran, T. M. Abdolkader, and N. Z. Butt, "Carrier-selective NiO/Si and TiO_2 /Si contacts for silicon heterojunction solar cells," *IEEE Trans. Electron Devices*, vol. 63, no. 9, pp. 3584–3590, Sep. 2016.

[20] J. Nelson, *Physics of Solar Cells*, 1st ed. London, U.K.: Imperial College Press, 2003.

[21] R. F. Pierret, *Advanced Semiconductor Fundamentals*, 2nd ed. Upper Saddle River, NJ, USA: Pearson Education, Inc., 2003.

[22] M. A. Green, "Accuracy of analytical expressions for solar cell fill factors," *Sol. Cells*, vol. 7, no. 3, pp. 337–340, Dec. 1982.

[23] Synopsys. (2013). *Synopsys TCAD, Release H-2013.03*. [Online]. Available: http://www.synopsys.com

[24] A. G. Aber, S. Glunz, and W. Warta, "Field effect passivation of high efficiency silicon solar cells," *Sol. Energy Mater. Sol. Cells*, vol. 29, no. 2, pp. 175–182, Mar. 1993.

[25] A. Metz, R. Meyer, B. Kuhlmann, M. Grauvogl, and R. Hezel, "18.5% efficient first-generation MIS inversion-layer silicon solar cells," in *Proc. Conf. Rec. 26th IEEE Photovolt. Spec. Conf.*, Oct. 1997, pp. 31–34.

[26] R. Schorner, R. Hezel, and R. Hezel, "High efficiency inversion layer solar cells on polycrystalline silicon by the application of silicon nitride," *IEEE Trans. Electron Devices*, vol. ED-28, no. 12, pp. 1466–1469, Dec. 1981.

[27] W. K. Metzger *et al.*, "Recombination kinetics and stability in polycrystalline Cu(In,Ga)Se_2 solar cells," *Thin Solid Films*, vol. 517, no. 7, pp. 2360–2364, Feb. 2009.

[28] W. Gerlach, H. Schlangenotto, and H. Maeder, "On the radiative recombination rate in silicon," *Phys. Status Solidi Appl. Mater. Sci.*, vol. 13, no. 1, pp. 277–283, Sep. 1972.

[29] M. A. Green, "Limits on the open-circuit voltage and efficiency of silicon solar cells imposed by intrinsic auger processes," *IEEE Trans. Electron Devices*, vol. ED-31, no. 5, pp. 671–678, May 1984.

[30] L. Chkoda *et al.*, "Work function of ITO substrates and band-offsets at the TPD/ITO interface determined by photoelectron spectroscopy," *Synth. Met.*, vols. 111–112, pp. 315–319, Jun. 2000.

Nithin Chatterji, photograph and biography not available at the time of publication.

Aldrin Antony, photograph and biography not available at the time of publication.

Pradeep R. Nair, photograph and biography not available at the time of publication.